Research article

Mengli Liu, Wenjun Liu*, Ximei Liu, Yuyi Ouyang, Huanran Hou, Ming Lei* and Zhiyi Wei

Yttrium oxide as a Q-switcher for the near-infrared erbium-doped fiber laser

https://doi.org/10.1515/nanoph-2019-0563
Received December 30, 2019; revised February 9, 2020; accepted February 9, 2020

Abstract: Yttrium oxide (Y_2O_3) has been widely used in metal-reinforced composites, microelectronics, waveguide lasers, and high-temperature protective coatings because of its good physical and photoelectric properties. However, few studies have been done on the nonlinear optical applications of Y_2O_3 as saturable absorbers (SAs) in fiber lasers so far. Here, a passively Q-switched near-infrared fiber laser using Y_2O_3 as a Q-switching device is demonstrated. The optical nonlinear properties of the Y_2O_3 SA prepared by the magnetron sputtering method were measured by the twin-detector measurement technique, and the modulation depth of the proposed Y_2O_3 SA was found to be 46.43%. The achieved Q-switched laser delivers an average output power of 26 mW at 1530 nm with a pulse duration of 592.7 ns. To the best of our knowledge, this is the first report on the optical nonlinearity of Y_2O_3 as a Q-switcher for the near-infrared fiber laser, which may deepen the understanding of the optical nonlinear properties of Y_2O_3 and make inroads into the potential market of optical modulation and optoelectronic devices.

***Corresponding authors: Wenjun Liu,** State Key Laboratory of Information Photonics and Optical Communications, School of Science, PO Box 91, Beijing University of Posts and Telecommunications, Beijing 100876, China; and Beijing National Laboratory for Condensed Matter Physics, Institute of Physics, Chinese Academy of Sciences, Beijing 100190, China, e-mail: jungliu@bupt.edu.cn. https://orcid.org/0000-0001-9380-2990; and **Ming Lei,** State Key Laboratory of Information Photonics and Optical Communications, School of Science, PO Box 91, Beijing University of Posts and Telecommunications, Beijing 100876, China, e-mail: mlei@bupt.edu.cn
Mengli Liu, Ximei Liu, Yuyi Ouyang and Huanran Hou: State Key Laboratory of Information Photonics and Optical Communications, School of Science, PO Box 91, Beijing University of Posts and Telecommunications, Beijing 100876, China
Zhiyi Wei: Beijing National Laboratory for Condensed Matter Physics, Institute of Physics, Chinese Academy of Sciences, Beijing 100190, China

Keywords: nonlinear optical materials; saturable absorbers; Q-switched laser; fiber lasers.

1 Introduction

Passively Q-switched fiber lasers (QSFL), which are generated by Q-factor modulation or intracavity loss regulation, have attracted much attention because of their intrinsic advantages of high energy, alignment-free structure, compactness, and high stability [1–4]. Up to now, QSFLs have been widely applied in medicine, industrial material processing, fiber-optical sensing, and optical communication [5–16]; but they can also be used as an ideal platform for investigating the dynamic evolution of solitons and saturated absorption of nanomaterials [17–33].

In recent years, passively QSFLs based on saturable absorbers (SAs) have received much attention. Semiconductor saturable absorber mirrors (SESAMs) are considered to be the hot topic in commercial applications. However, the inevitable features of complex manufacturing process, narrow bandwidth, and high cost make it hard for them to meet future commercial application requirements [34, 35]. Graphene, which has emerged as required by time, has been attracting growing attention in recent years. The characteristics of ultra-broadband absorption and ultrafast electron dynamics make it shine brilliantly in the field of optoelectronics [36, 37]. The tremendous success of graphene has also led to the exploration of more potential materials [38–42]. Transition-metal dichalcogenides (TMDs) possess unique photoelectric properties that vary with thickness. They not only exhibit ultra-wideband absorption characteristics due to defective states but also have outstanding performance in realizing ultrafast lasers [43–45]. Similarly, topological insulators (TIs) and black phosphorous (BP) have recently got breakthroughs in applications of photonics and photoelectronics in the near-infrared band [46–49]. In addition, more new materials with excellent properties are beginning to emerge [50–52].

Yttrium oxide (Y_2O_3) performs well in terms of hardness, melting point, and chemical stability. Therefore, it is

often used in metal-reinforced composites, microelectronics, waveguide lasers, and high-temperature protective coatings [53–55]. In microelectronics, Y_2O_3 is considered as a potential gate dielectric material because of its high dielectric constant and good compatibility with silicon [56]. Moreover, because of the excellent thermo-optical properties of Y_2O_3, it can be easily doped with a variety of rare earth ions, thus helping to produce high-power waveguide lasers [57, 58]. However, few studies have been done on the nonlinear optical applications of Y_2O_3 as SAs in fiber lasers so far.

In order to stimulate the application of Y_2O_3 in more fields, we attempted to explore its optical nonlinearity. Combined with the common magnetron sputtering method, the tapered Y_2O_3 SA was prepared. By coupling the Y_2O_3 SA into the cavity, a QSFL delivering an average output power of 26 mW at 1530 nm with a pulse duration of 592.7 ns was obtained. Our experiments not only prove the optical nonlinearity of Y_2O_3 but also provide the possibility for the further development of optical modulation and optoelectronic devices.

2 Preparation and characterization of Y_2O_3 SA

To enhance the nonlinearity and reduce thermal damage of the Y_2O_3 SA, the tapered fiber structure was selected. Meanwhile, to ensure convenience and efficiency of production, we chose the appropriate production method, namely magnetron sputtering deposition (MSD). The clean, tapered optical fiber, which was prepared in advance, had a waist diameter of 14 μm and effective fused zone length of 0.8 cm; the large effective length of the fused zone and the small waist diameter of the tapered fiber help in enhancing the nonlinearity of the Y_2O_3 SA. The specific production process is as follows: First, the commercially purchased Y_2O_3 target with 99.99% purity was tapered and fixed in a vacuum chamber. A vacuum pump was used to bring the degree of vacuum to 10×10^{-3} Pa. Then, excited and accelerated Ar ions were made to bombard the Y_2O_3 target under the action of an electric field. Subsequently, the sputtered Y_2O_3 particles were uniformly deposited on the outer wall of the optical fiber. Meanwhile, the fiber was rotated evenly at a speed of 10 rpm to make the material dense and uniform. The flow rate of Ar was 20 sccm (standard cubic centimeter per minute) during the the sputtering process. The temperature of the preparation process was 200°C.

After the preparation of the Y_2O_3 SA, some necessary characterization and measurements were carried out. Atomic force microscopy (AFM) was used to examine the surface properties of the prepared Y_2O_3 SA (Figure 1). By detecting the thickness difference between the material coverage area and the silicon substrate in Figure 1A, the exact thickness of Y_2O_3 was estimated as 7 nm in Figure 1B. According to the definition of two-dimensional (2D) materials, the Y_2O_3 used here can be considered as two dimensional [59, 60]. Meanwhile, the surface morphology of Y_2O_3 is shown in Figure 1C, which reveals the compactness and uniformity of the material surface.

X-ray photoelectron spectroscopy (XPS) is able to effectively determine the composition and properties of materials. As shown in Figure 2A, the prominent O-Y, Y-O-Si, and O-Si peaks are located at 529.8, 531.9, and 532.9 eV, respectively. The Y-O-Si peak that is observed in the film may be the result of diffusion of the substrate silicon [61]. As shown in Figure 2B, the prominent Y $3d_{5/2}$ and Y $3d_{3/2}$ peaks are located at 157 and 159 eV, respectively. The XPS spectrum of Y_2O_3 is highly consistent with those obtained in previous studies [61, 62]. The agreement in both composition and binding energy proves the existence of Y_2O_3.

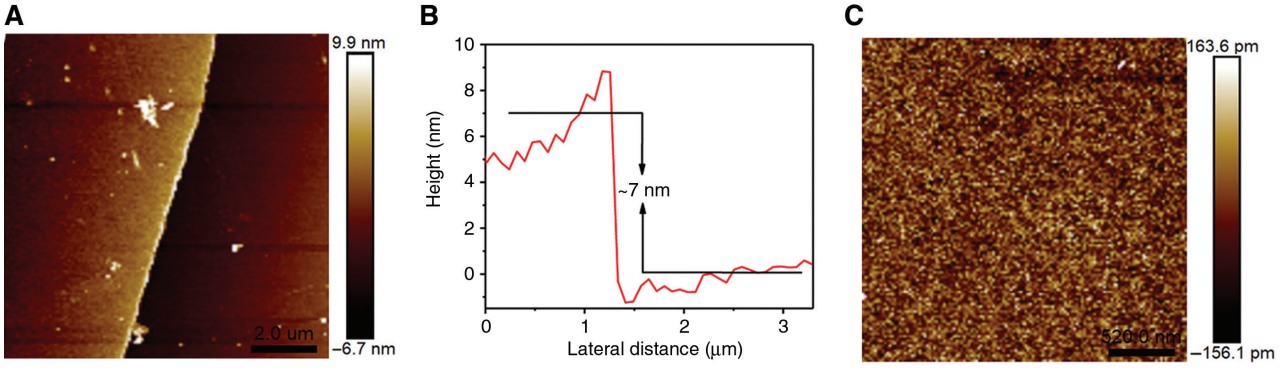

Figure 1: The AFM of Y_2O_3.
(A) Material boundary, (B) thickness, and (C) surface morphology of Y_2O_3.

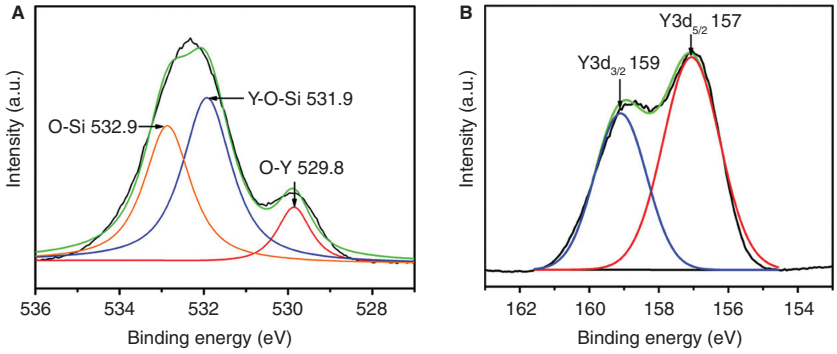

Figure 2: The XPS of Y_2O_3 film.
(A) O 1s spectra of Y_2O_3 films. (B) Y 3d spectra of Y_2O_3 films.

The absorption spectrum of Y_2O_3 is shown in Figure 3A, which indicates that the as-prepared Y_2O_3 has ultrawide absorption characteristics. The absorptivity of the fabricated Y_2O_3 was measured as 38.346% at 1550 nm. In the investigation of the optical nonlinearity of Y_2O_3, the twin-detector measurement technique was used. The light transmissions of Y_2O_3 at different powers were recorded separately, which are shown in the figure as blue points. The pump source during the measurement was operated at 1550 nm, and the corresponding pulse duration and repetition rate were 700 fs and 120 MHz, respectively. The results were fitted by

$$T = 1 - \left(\frac{\alpha_s}{1 + I/I_{sat}} + \alpha_{ns} \right).$$

The results of curve-fitting in Figure 3B show that the Y_2O_3 SA has a modulation depth (α_s) of 46.43%, nonsaturable loss (α_{ns}) of 26.75%, and saturable intensity (I_{sat}) of 1.58 MW/cm^2. The large modulation depth may come from two aspects: the strong nonlinearity of the Y_2O_3 material itself, and the small waist diameter and large effective length of the fused zone of the tapered fiber. The performance comparison of the Y_2O_3 SA and other nanomaterial-based SAs is shown in Table 1. The relatively large modulation depth of the Y_2O_3 SA is beneficial to the generation of ultrashort pulses. Meanwhile, the small saturation intensity of the Y_2O_3 SA is conducive to a low start threshold of the Q-switched laser. The insertion loss (IL) of the Y_2O_3 SA is 1.4 dB, which is the average value.

3 Experiment

Considering the superiority of the fiber laser in terms of alignment-free structure, compactness, and high stability, it was chosen as the platform for the nonlinearity verification of Y_2O_3. Figure 4 is the device diagram of a commonly used ring-cavity fiber laser. The length of the erbium-doped fiber (EDF) used as the gain medium is 60 cm, and the total length of the cavity is 2.1 m. The source in the cavity is a commercial laser pump operating at 980 nm. As an important device for coupling the light source into the cavity, the wavelength division multiplexer (WDM, 980/1550nm) can combine optical signals of different wavelengths into one bundle. The isolator (ISO) ensures the unidirectional transmission of light, thereby guaranteeing the normal operation of the laser and avoiding unnecessary device damage. The intracavity

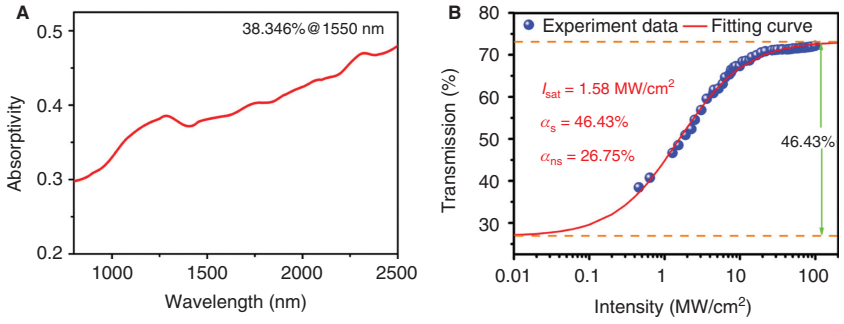

Figure 3: Linear and nonlinear absorption characterization of Y_2O_3.
(A) Absorption spectrum of Y_2O_3 films. (B) Nonlinear absorption characteristics of the Y_2O_3 SA.

Table 1: Nonlinear behavior of some SAs.

Materials	Modulation depth (%)	Saturation intensity (MW/cm²)	Unsaturated loss (%)	IL (dB)	Refs.
Graphene	1.5	–	–	0.5	[63]
BP	18.55	10.74	~46	2.7	[64]
Bi_2Te_3	22	57	21	1	[65]
WS_2	4.85	3.83	3.65	0.2	[66]
MoS_2	2	~10	48.5	2.9	[67]
Y_2O_3	46.43	1.58	26.75	1.4	This work

IL, insertion loss.

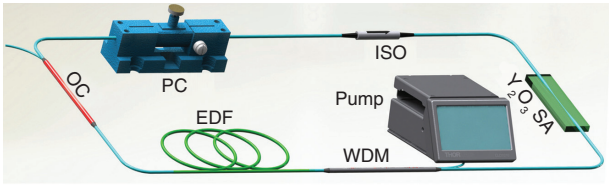

Figure 4: Experimental installation diagram of the proposed fiber laser.

birefringence and polarization state are adjusted by a polarization controller (PC), thus optimizing the operating state for a stable pulse output. With an 80:20 optical coupler (OC), 20% of the intracavity signals are exported for real-time monitoring. The Y_2O_3 SA is placed between the WDM and ISO. Optical devices such as an oscilloscope (Tektronix DPO 3054) and an optical spectrum analyzer (Yokogawa AQ 6370C) outside the cavity are used to monitor and measure the real-time dynamics in the cavity.

4 Results and discussion

After inserting the Y_2O_3 SA into the cavity, stable Q-switched pulses appeared at the pump power of 148 mW. The pulse sequences at different pump powers are shown in Figure 5A. In Figure 5B, the spectrum of the realized Q-switched operation has a central wavelength of 1530 nm with a bandwidth of 1.5 nm. It is worth mentioning that there is no significant change in the spectral shape recorded at different time intervals. Meanwhile, there is no remaining pump power from the output. The monopulse envelope of the output pulse at 630 mW is shown in Figure 5C, whose typical symmetrical Gaussian shape shows a pulse duration of 592.7 ns. The radio frequency (RF) spectrum measured is shown in Figure 5D. At the resolution bandwidth of 10 Hz, the Q-switched system exhibits a signal-to-noise ratio (SNR) of 65 dB. Meanwhile, the frequency-doubled signal decreased evenly over a wide range of frequencies, which further proved the stability of the system.

With the increase of input power, the repetition rate of output pulse increases almost uniformly in the range 112–217 kHz, as shown in Figure 6A. The pulse duration decreases rapidly in the initial stage of power growth and tends to be stable in the later stage, which is related to the pump-induced gain compression effect as confirmed in Ref. [68]. The stability of the later pulse duration indicates that the absorber tends toward saturation. The adjustable range of pulse duration is 2259–592.7 ns when input power changes from 148 to 630 mW. The repetition rate of the Q-switched pulse increases with the increase of the pump power as reported in Ref. [69]. From Figure 6B, for a pump power of 630 mW, the average output power and pulse energy are 26 mW and 120 nJ, respectively. It is worth mentioning that at the maximum pump power, the growth trend of the average output power is still upward, which indicates that the stable working condition can be maintained even at high power. The maximum damage threshold of the Y_2O_3 SA is ~68 mJ/cm². In the experiment, mode-locking was not obtained because the nonlinearity and anomalous dispersion did not reach equilibrium in this case. Attempts to apply the Y_2O_3 SA in mode-locked lasers will continue in future work.

The comparison between the proposed QSFL and previous lasers is shown in Table 2. The pulse duration of 592.7 ns is proved to be competitive among SA-based QSFLs. Moreover, the high melting point and good chemical stability of the Y_2O_3 enable the Q-switched oscillator in maintaining stable, high power. Therefore, the Y_2O_3 SA may make inroads into the potential market of optical modulation and optoelectronic devices.

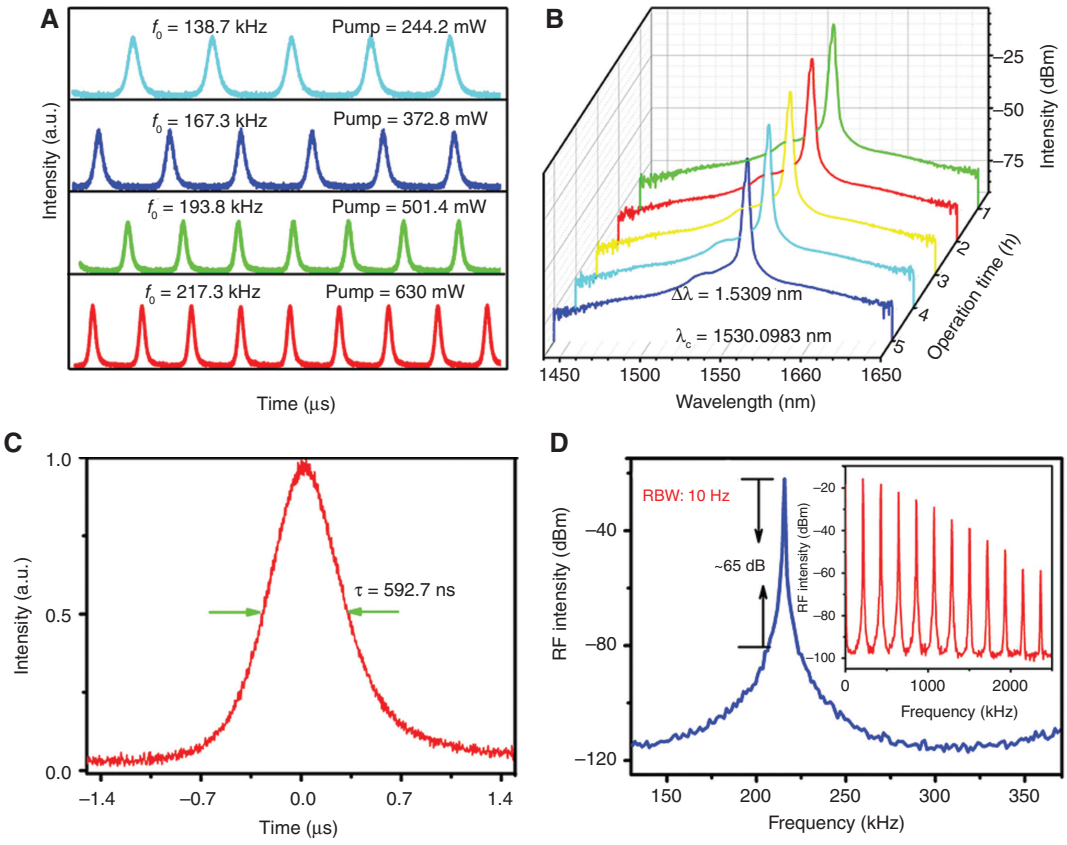

Figure 5: Performance of QSFL based on Y_2O_3 SA.
(A) Pulse sequence at different pump powers. (B) Spectra for different time periods. (C) Pulse duration of 592.7 ns. (D) RF spectrum.

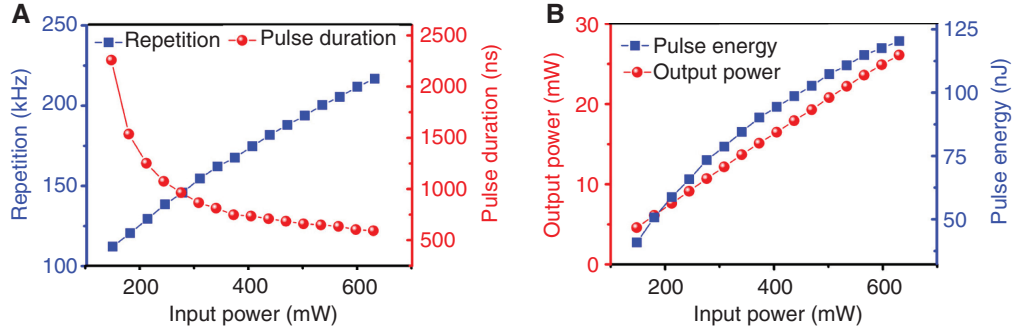

Figure 6: Characteristics of proposed QSFL variation under different power.
(A) Pulse duration and repetition rate as functions of input power. (B) Average output power and pulse energy as functions of input power.

Table 2: Performance comparison of SA-based QSFLs.

Materials	$\Delta\lambda/\lambda$ (nm)	Freqency (kHz)	τ (μs)	P (mW)	Energy (nJ)	SNR (dB)	Refs.
Graphene	0.02/1539.6	10.36–41.8	3.89	<1.2	28.7	30	[63]
BP	0.2/1562.87	6.983–15.78	13.2	~1.5	94.3	45	[64]
Bi_2Se_3	0.45/1566.9	2.154–12.82	16.3	20	1525	36.4	[65]
WS_2	–/1558	79–97	1.3	16.4	179.6	44	[66]
MoS_2	–/1551.2	8.77–43.47	3.3	5.91	160	50	[67]
Y_2O_3	1.5/1530	112–217	0.5927	26	120	65	This work

5 Conclusion

An erbium-doped QSFL using Y_2O_3 as the Q-switched device to deliver nanosecond pulses has been demonstrated in this article. The generated stable Q-switched pulses have a controlled repetition rate of 112–217 kHz, pulse duration of 593 ns, output power of 26 mW, and pulse energy of 120 nJ. The pulse duration of 593 ns is comparable with that of other SA-based QSFLs. Moreover, the high melting point and good chemical stability Y_2O_3 result in improved stability of the laser even at high power. Our experiments have shown that the Y_2O_3 SA not only has strong nonlinearity and advantages in achieving ultrashort pulse duration but also has worked steadily in high-power operation. Therefore, the Y_2O_3 SA may make inroads into the potential market of optical modulation and optoelectronic devices.

Acknowledgment: This work was supported by the National Natural Science Foundation of China (11674036, 11875008, 91850209, Funder Id: http://dx.doi.org/10.13039/501100001809), the Beijing Youth Top-notch Talent Support Program (2017000026833ZK08), the Fund of State Key Laboratory of Information Photonics and Optical Communications (Beijing University of Posts and Telecommunications (IPOC2019ZZ01), the Fundamental Research Funds for the Central Universities (500419305), the State Key Laboratory of Advanced Optical Communication Systems and Networks, Shanghai Jiao Tong University (2019GZKF03007), and the Beijing University of Posts and Telecommunications Excellent Ph.D. Students Foundation (CX2019202).

References

[1] Woodward RI, Kelleher EJR, Howe RCT, et al. Tunable Q-switched fiber laser based on saturable edge-state absorption in few-layer molybdenum disulfide (MoS_2). Opt Express 2014;22:31113–22.
[2] Liu W, Liu M, Han H, et al. Nonlinear optical properties of WSe_2 and $MoSe_2$ films and their applications in passively Q-switched erbium doped fiber lasers. Photon Res 2018;6:C15–21.
[3] Liu ML, Ouyang YY, Hou HR, Liu WJ. Q-switched fiber laser operating at 1.5 μm based on WTe_2. Chin Opt Lett 2019;17:020006.
[4] Liu ML, OuYang YY, Hou HR, Lei M, Liu WJ, Wei ZY. MoS_2 saturable absorber prepared by chemical vapor deposition method for nonlinear control in Q-switching fiber laser. Chin Phys B 2018;27:084211.
[5] Rizvi NH. Femtosecond laser micromachining: current status and applications. RIKEN Rev 2003;50:107–12.
[6] Merker M, Ackermann R, Kammel R, Kunert KS, Nolte S. An in vitro study on focusing fs-laser pulses into ocular media for ophthalmic surgery. Laser Surg Med 2013;45:589–96.
[7] Morin F, Druon F, Hanna M, Georges P. Microjoule femtosecond fiber laser at 1.6 μm for corneal surgery applications. Opt Lett 2009;34:1991–3.
[8] Yun SH, Boudoux C, Pierce MC, De Boer JF, Tearney GJ, Bouma BE. Extended-cavity semiconductor wavelength-swept laser for biomedical imaging. IEEE Photon Technol Lett 2004;16:293–5.
[9] Xu C, Wise FW. Recent advances in fibre lasers for nonlinear microscopy. Nat Photon 2013;7:875–82.
[10] Huang W, Xie Z, Fan T, et al. Black-phosphorus-analogue tin monosulfide: an emerging optoelectronic two-dimensional material for high-performance photodetection with improved stability under ambient/harsh conditions. J Mater Chem C 2018;6:9582–93.
[11] Xie Z, Wang D, Fan T, et al. Black phosphorus analogue tin sulfide nanosheets: synthesis and application as near-infrared photothermal agents and drug delivery platforms for cancer therapy. J Mater Chem B 2018;6:4747–55.
[12] Fan T, Xie Z, Huang W, Li Z, Zhang H. Two-dimensional non-layered selenium nanoflakes: facile fabrications and applications for self-powered photo-detector. Nanotechnology 2019;30:114002.
[13] Xing C, Huang W, Xie Z, et al. Ultrasmall bismuth quantum dots: facile liquid-phase exfoliation, characterization, and application in high-performance UV-Vis photodetector. ACS Photon 2018;5:621–9.
[14] Xie Z, Chen S, Duo Y, et al. Biocompatible two-dimensional titanium nanosheets for multimodal imaging-guided cancer theranostics. ACS Appl Mater Interf 2019;11:22129–40.
[15] Xie Z, Peng YP, Yu L, et al. Solar-inspired water purification based on emerging two-dimensional materials: status and challenges. Sol RRL 2020;4:1900400.
[16] Liang X, Ye X, Wang C, et al. Photothermal cancer immunotherapy by erythrocyte membrane-coated black phosphorus formulation. J Control Release 2019;296:150–61.
[17] Mao D, Zhang S, Wang Y, et al. WS_2 saturable absorber for dissipative soliton mode locking at 1.06 and 1.55 μm. Opt Express 2015;23:27509–19.
[18] Sun Z, Martinez A, Wang F. Optical modulators with 2D layered materials. Nat Photon 2016;10:227–38.
[19] Yan P, Liu A, Chen Y, et al. Passively mode-locked fber laser by a cell-type WS_2 nanosheets saturable absorber. Sci Rep 2015;5:12587.
[20] Zhang H, Tang DY, Zhao LM, Bao QL, Loh KP. Large energy mode locking of an erbium-doped fiber laser with atomic layer graphene. Opt Express 2009;17:17630–5.
[21] Wu K, Guo C, Wang H, Zhang X, Wang J, Chen J. All-optical phase shifter and switch near 1550nm using tungsten disulfide (WS_2) deposited tapered fiber. Opt Express 2017;25:17639–49.
[22] Luo Z, Huang Y, Zhong M, et al. 1-, 1.5-, and 2-μm fiber lasers Q-switched by a broadband few-layer MoS_2 saturable absorber. J Lightwave Technol 2014;32:4077–84.
[23] Liu W, Pang L, Han H, Bi K, Lei M, Wei Z. Tungsten disulphide for ultrashort pulse generation in all-fiber lasers. Nanoscale 2017;9:5806–11.
[24] Zhang M, Howe RCT, Woodward RI, et al. Solution processed MoS_2-PVA composite for sub-bandgap mode-locking of a wideband tunable ultrafast Er: fiber laser. Nano Res 2015;8:1522–34.
[25] Liu WJ, Zhu YN, Liu ML, et al. Optical properties and applications for MoS_2-Sb_2Te_3-MoS_2 heterostructure materials. Photon Res 2018;6:220–7.

[26] Song Y, Shi X, Wu C, Tang D, Zhang H. Recent progress of study on optical solitons in fiber laser. Appl Phys Rev 2019;6:021313.
[27] Song Y, Liang Z, Zhang H, et al. Period-doubling and quadrupling bifurcation of vector soliton bunches in a graphene mode locked fiber laser. IEEE Photon J 2017;9:4502308.
[28] Xie Z, Xing C, Huang W, et al. Ultrathin 2D nonlayered tellurium nanosheets: facile liquid-phase exfoliation, characterization, and photoresponse with high performance and enhanced stability. Adv Funct Mater 2018;28:1705833.
[29] Xie Z, Zhang F, Liang Z, et al. Revealing of the ultrafast third-order nonlinear optical response and enabled photonic application in two-dimensional tin sulfide. Photon Res 2019;7:494–502.
[30] Wu L, Xie Z, Lu L, et al. Few-layer tin sulfide: a promising black-phosphorus-analogue 2D material with exceptionally large nonlinear optical response, high stability, and applications in all-optical switching and wavelength conversion. Adv Opt Mater 2018;6:1700985.
[31] Xing C, Xie Z, Liang Z, et al. 2D nonlayered selenium nanosheets: facile synthesis, photoluminescence, and ultrafast photonics. Adv Opt Mater 2017;5:1700884.
[32] Zhang Y, Lim CK, Dai Z, et al. Photonics and optoelectronics using nano-structured hybrid perovskite media and their optical cavities. Phys Rep 2019;795:1–51.
[33] Guo S, Zhang Y, Ge Y, Zhang S, Zeng H, Zhang H. 2D V-V binary materials: status and challenges. Adv Mater 2019;31:1902352.
[34] Keller U, Weingarten KJ, Kartner FX, et al. Semiconductor saturable absorber mirrors (SESAM's) for femtosecond to nanosecond pulse generation in solid-state laser. IEEE J Sel Top Quantum Electron 1996;2:435–53.
[35] Okhotnikov O, Grudinin A, Pessa M. Ultra-fast fibre laser systems based on SESAM technology: new horizons and applications. New J Phys 2004;6:177.
[36] Bao QL, Zhang H, Wang Y, et al. Atomic-layer graphene as a saturable absorber for ultrafast pulsed lasers. Adv Funct Mater 2009;19:3077–83.
[37] Zhang M, Kelleher EJR, Torrisi F, et al. Tm-doped fiber laser mode-locked by graphene-polymer composite. Opt Express 2012;20:25077–84.
[38] Guo B, Wang SH, Wu ZX, et al. Sub-200 fs soliton mode-locked fiber laser based on bismuthene saturable absorber. Opt Express 2018;26:22750–60.
[39] Song YF, Shi XJ, Wu CF, Tang DY, Zhang H. Recent progress of study on optical solitons in fiber lasers. Appl Phys Rev 2019;6:021313.
[40] Jiang YQ, Miao LL, Jiang GB, et al. Broadband and enhanced nonlinear optical response of MoS_2/graphene nanocomposites for ultrafast photonics applications. Sci Rep 2015;5:16372.
[41] Song YF, Liang ZM, Jiang XT, et al. Few-layer antimonene decorated microfiber: ultra-short pulse generation and all-optical thresholding with enhanced long term stability. 2D Mater 2017;4:045010.
[42] Xing CY, Jing GH, Liang X, et al. Graphene oxide/black phosphorus nanoflake aerogels with robust thermo-stability and significantly enhanced photothermal properties in air. Nanoscale 2017;9:8096–101.
[43] Liu M, Liu W, Wei Z. $MoTe_2$ saturable absorber with high modulation depth for erbium-doped fiber laser. J Lightwave Technol 2019;37:3100–5.
[44] Liu W, Liu M, OuYang Y, Hou H, Lei M, Wei ZY. CVD-grown $MoSe_2$ with high modulation depth for ultrafast mode-locked erbium-doped fiber laser. Nanotechnology 2018;29:394002.
[45] Liu WJ, Liu ML, Liu B, et al. Nonlinear optical properties of MoS_2-WS_2 heterostructure in fiber lasers. Opt Express 2019;27:6689–99.
[46] Zhao C, Zhang H, Qi X, et al. Ultra-short pulse generation by a topological insulator based saturable absorber. Appl Phys Lett 2012;101:211106.
[47] Sotor J, Sobon G, Macherzynski W, Paletko P, Grodecki K, Abramski KM. Mode-locking in Er-doped fiber laser based on mechanically exfoliated Sb_2Te_3 saturable absorber. Opt Express 2014;4:1–6.
[48] Na D, Park K, Park KH, Song YW. Passivation of black phosphorus saturable absorbers for reliable pulse formation of fiber lasers. Nanotechnology 2017;28:475207.
[49] Wu K, Chen B, Zhang X, et al. High-performance mode-locked and Q-switched fiber lasers based on novel 2D materials of topological insulators, transition metal dichalcogenides and black phosphorus: review and perspective. Opt Commun 2018;406:214–29.
[50] Liu WJ, Liu ML, Chen X, et al. Ultrafast photonics of two dimensional $AuTe_2Se_{4/3}$ in fiber lasers. Commun Phys 2020;3:15.
[51] Liu WJ, Liu ML, Liu XM, Lei M, Wei ZY. SnSSe as a saturable absorber for an ultrafast laser with superior stability. Opt Lett 2020;45:419–2.
[52] Liu WJ, Liu ML, Lin S, et al. Synthesis of high quality silver nanowires and their applications in ultrafast photonics. Opt Express 2019;27:16440–8.
[53] Shim JH, Chao CC, Huang H, Prinz FB. Atomic layer deposition of yttria-stabilized zirconia for solid oxide fuel cells. Chem Mater 2007;19:3850–4.
[54] Huang H, Nakamura M, Su P, Fasching R, Saito Y, Prinz FB. High-performance ultrathin solid oxide fuel cells for low-temperature operation. J Electrochem Soc 2007;154:B20–4.
[55] Zhu S, Zu XT, Wang LM, Ewing RC. Nanodomains of pyrochlore formed by Ti ion implantation in yttria-stabilized zirconia. Appl Phys Lett 2002;80:4327–9.
[56] Robertson J. Band offsets of wide-band-gap oxides and implications for future electronic devices. J Vac Sci Technol B 2000;18:1785–91.
[57] Choudhary A, Dhingra S, D'Urso B, et al. Q-switched operation of a pulsed-laser-deposited Yb: Y_2O_3 waveguide using graphene as a saturable absorber. Opt Lett 2014;39:4325–8.
[58] Szela JW, Sloyan KA, Parsonage TL, Mackenzie JI, Eason RW. Laser operation of a Tm: Y_2O_3 planar waveguide. Opt Express 2013;21:12460–8.
[59] Lin YH, Cheng CK, Chen KH, et al. Single-crystal Y_2O_3 epitaxially on GaAs (001) and (111) using atomic layer deposition. Materials 2015;8:7084–93.
[60] Li Y, Hao J, Song H, et al. Selective light absorber-assisted single nickel atom catalysts for ambient sunlight-driven CO_2 methanation. Nat Commun 2019;10:2359.
[61] Zhu J, Zhu Y, Shen W, et al. Growth and characterization of yttrium oxide films by reactive magnetron sputtering. Thin Solid Films 2011;519:4894–8.
[62] Cheng XR, Qi ZM, Zhang GB, Zhou HJ, Zhang WP, Yin M. Growth and characterization of Y_2O_3 thin films. Physica B 2009;404:146–9.

[63] Wang J, Luo Z, Zhou M, et al. Evanescent-light deposition of graphene onto tapered fibers for passive Q-switch and mode-locker. IEEE Photon J 2012;4:1295–305.
[64] Chen Y, Jiang G, Chen S, et al. Mechanically exfoliated black phosphorus as a new saturable absorber for both Q-switching and mode-locking laser operation. Opt Express 2015;23:12823–33.
[65] Chen Y, Zhao C, Chen S, et al. Large energy, wavelength widely tunable, topological insulator Q-switched erbium doped fiber laser. IEEE J Sel Top Quan 2014;20:315–22.
[66] Zhang M, Hu G, Hu G, et al. Yb- and Er-doped fber laser Q-switched with an optically uniform, broadband WS_2 saturable absorber. Sci Rep 2015;5:17482.
[67] Huang Y, Luo Z, Li Y, et al. Widely-tunable, passively Q-switched erbium-doped fiber laser with few-layer MoS_2 saturable absorber. Opt Express 2014;22: 25258–66.
[68] Herda R, Kivistö S, Okhotnikov OG. Dynamic gain induced pulse shortening in Q-switched lasers. Opt Lett 2008;33:1011–3.
[69] Lecourt JB, Martel G, Guézo M, Labbé C, Loualiche S. Erbium-doped fiber laser passively Q-switched by an InGaAs/InP multiple quantum well saturable absorber. Opt Commun 2006;263:71–83.